Molecular Systems Biology 3; Article number 112; doi:10.1038/msb4100153
Citation: ***Molecular Systems Biology*** **3:112**

www.molecularsystemsbiology.com

molecular systems biology

A top-down systems biology view of microbiome-mammalian metabolic interactions in a mouse model

François-Pierre J Martin[1,2], Marc-Emmanuel Dumas[1], Yulan Wang[1], Cristina Legido-Quigley[1], Ivan KS Yap[1], Huiru Tang[1,3], Séverine Zirah[1,4], Gerard M Murphy[1], Olivier Cloarec[1], John C Lindon[1], Norbert Sprenger[2], Laurent B Fay[2], Sunil Kochhar[2], Peter van Bladeren[2], Elaine Holmes[1] and Jeremy K Nicholson[1,*]

[1] Department of Biomolecular Medicine, Division of Surgery, Oncology, Reproductive Biology and Anaesthetics, Faculty of Medicine, Imperial College London, South Kensington, London, UK and [2] Nestlé Research Center, Vers-chez-les-Blanc, Lausanne, Switzerland
[3] Present address: State Key Laboratory of Magnetic Resonance and Atomic and Molecular Physics, Wuhan Centre for Magnetic Resonance, Wuhan Institute of Physics and Mathematics, The Chinese Academy of Sciences, Wuhan 430071, PR China
[4] Present address: Regulations, Development and Molecular Diversity, National Museum of Natural History, Paris 75005, France
* Corresponding author. Department of Biomolecular Medicine, Division of Surgery, Oncology, Reproductive Biology and Anaesthetics, Faculty of Medicine, Imperial College London, Sir Alexander Fleming Building, Exhibition road, South Kensington, London SW7 2AZ, UK. Tel.: +44 20 7594 3195; Fax: +44 20 7594 3226; E-mail: j.nicholson@imperial.ac.uk

Received 5.2.07; accepted 14.3.07

Symbiotic gut microorganisms (microbiome) interact closely with the mammalian host's metabolism and are important determinants of human health. Here, we decipher the complex metabolic effects of microbial manipulation, by comparing germfree mice colonized by a human baby flora (HBF) or a normal flora to conventional mice. We perform parallel microbiological profiling, metabolic profiling by ^{1}H nuclear magnetic resonance of liver, plasma, urine and ileal flushes, and targeted profiling of bile acids by ultra performance liquid chromatography–mass spectrometry and short-chain fatty acids in cecum by GC-FID. Top-down multivariate analysis of metabolic profiles reveals a significant association of specific metabotypes with the resident microbiome. We derive a transgenomic graph model showing that HBF flora has a remarkably simple microbiome/metabolome correlation network, impacting directly on the host's ability to metabolize lipids: HBF mice present higher ileal concentrations of tauro-conjugated bile acids, reduced plasma levels of lipoproteins but higher hepatic triglyceride content associated with depletion of glutathione. These data indicate that the microbiome modulates absorption, storage and the energy harvest from the diet at the systems level.
Molecular Systems Biology 22 May 2007; doi:10.1038/msb4100153
Subject Categories: metabolic and regulatory networks; molecular biology of disease
Keywords: co-metabolism; gut microflora; metabonomics/metabolomics; network modeling; systems biology

Introduction

The symbiotic gut microbiome exerts a strong influence on the metabolic phenotype of the mammalian host and participates in extensive microbial–mammalian co-metabolism (Dunne, 2001; Xu and Gordon, 2003; Backhed *et al*, 2005; Eckburg *et al*, 2005; Holmes and Nicholson, 2005; Nicholson *et al*, 2005; Gill *et al*, 2006; Martin *et al*, 2006; Nicholson, 2006; Turnbaugh *et al*, 2006). Gut microbial composition is now known to vary significantly in obese animal (Turnbaugh *et al*, 2006) and human (Ley *et al*, 2006) populations, and recent studies have shown that the exact state of the gut microbial ecology and metabolic activities may be of fundamental importance in the control of calorific absorption (Xu *et al*, 2003; Backhed *et al*, 2004) and in the development of insulin resistance and nonalcoholic fatty liver disease in high-fat-diet experiments (Dumas *et al*, 2006). We know that the symbiotic gut microbiome acts as an extended genome (Lederberg, 2000) and has evolved to exert control on a number of important mammalian metabolic regulatory functions (Dunne, 2001; Pereira and Gibson, 2002; Xu and Gordon, 2003; Xu *et al*, 2003; Backhed *et al*, 2004, 2005; Holmes and Nicholson, 2005; Nicholson *et al*, 2005; Dumas *et al*, 2006; Gill *et al*, 2006; Martin *et al*, 2006; Sonnenburg *et al*, 2006). Gut microbes extensively co-metabolize bile acids and these have mammalian endocrine functions (Houten *et al*, 2006; Watanabe *et al*, 2006).

The integrated metabolism of the bile acid pools in mammals is a good example of the complex transgenomic

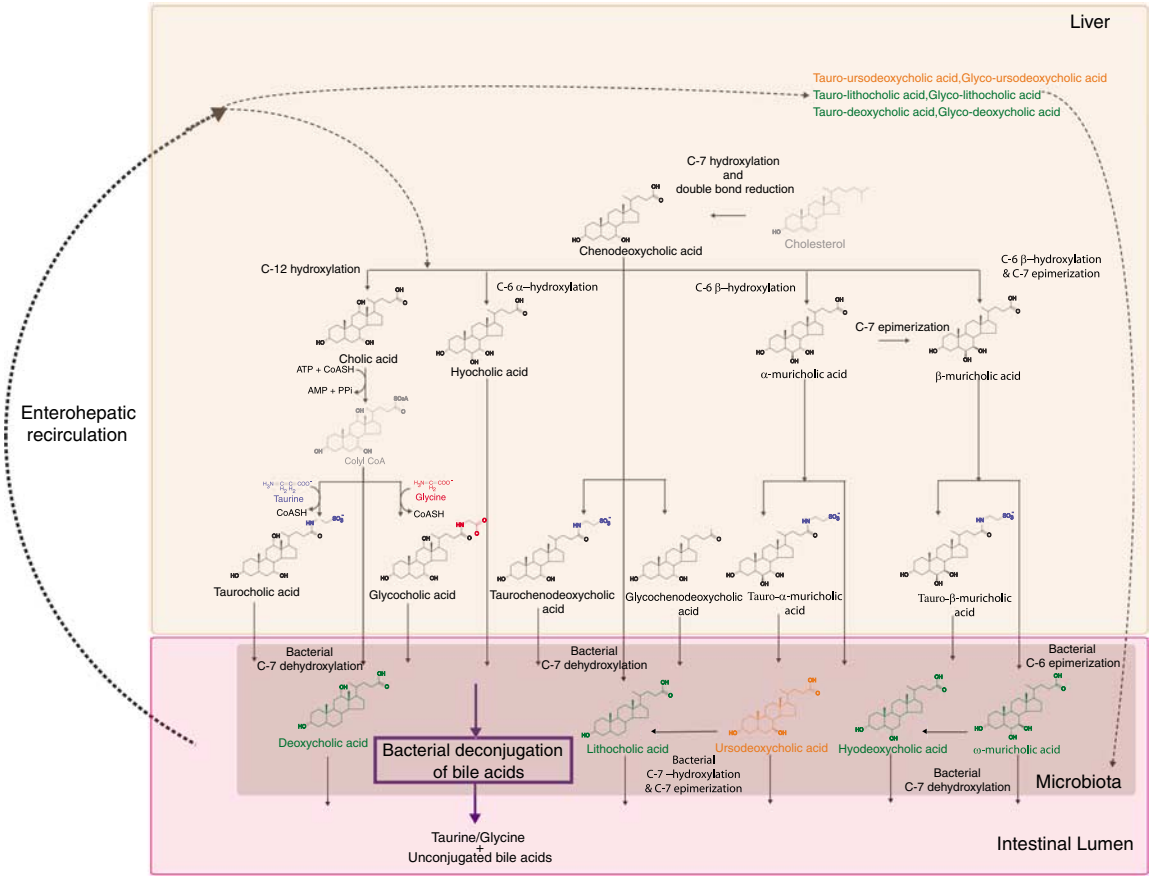

Figure 1 Metabolism and synthesis of the major bile acids in mouse. Key: Color denotes family of bile acids, that is, primary bile acids synthesized in liver in black, secondary bile acids synthesized in liver and processed by microflora in green and tertiary bile acids synthesized in liver, processed by microflora and re-metabolized in liver through enterohepatic recirculation in orange. Conjugation with taurine and glycine is colored in blue and red respectively. Key intermediates in the pathway are colored in gray.

biochemical interactions between host and microbiome symbionts as summarized in Figure 1. Bile acids are synthesized from cholesterol in the liver by a multi-enzyme coordinated process (Palmeira and Rolo, 2004) and are crucial for the absorption of dietary fats and lipid-soluble vitamins in the intestine (Staggers *et al*, 1982). Bile acids also have a role in maintaining the intestinal barrier function to prevent intestinal bacterial overgrowth and translocation (Lorenzo-Zuniga *et al*, 2003; Ogata *et al*, 2003), as well as invasion of underlying tissues by enteric bacteria (Ogata *et al*, 2003). In addition, abnormal bile acid profiles are indicative of various hepato-gastrointestinal diseases, such as dietary fat malabsorption and gallstone formation (Chace, 2001; Ijare *et al*, 2005) and might have an essential role in regulating obesity or type II diabetes (Houten *et al*, 2006; Watanabe *et al*, 2006). Many so-called secondary bile acids (deoxycholic, lithocholic, hyodeoxycholic and ω-muricholic acids) can be regarded as examples of mammalian-microbiotal co-metabolism (Nicholson *et al*, 2005) and have different metabolic fates via enterohepatic recirculation (Nicholson *et al*, 2004). This is part of what we term the microbiome–host metabolic axis, which we define here for the first time as 'the multi-way exchange and co-metabolism of compounds between the host organism and the gut microbiome resulting in transgenomically regulated secondary metabolites, which have biological activity in both host and microbial compartments'. Understanding the effects of bacterial metabolism on the balance of bile acids in enterohepatic recirculation is a major challenge owing to the implications of microbiota in fat absorption, lipid metabolism, drug therapeutic or toxic effects as well as direct effects within the gastrointestinal tract and its contents (Van *et al*, 2002). In this regard, recent advances in microbial and metabolic profiling now enable the multi-compartment study of bile acids and their effect on intermediary metabolism.

The application of high-resolution ^{1}H nuclear magnetic resonance (NMR) spectroscopy of biofluids and tissues coupled with multivariate statistical methods is a well-established tool for untargeted metabolic profiling (Nicholson and Wilson, 1989; Nicholson *et al*, 2002, 2005; Wang *et al*, 2005). Hyphenated chromatographic-mass spectrometric methods such as ultra-performance liquid chromatography–mass spectrometry (UPLC–MS)-based profiling techniques have also been recently used effectively for functional genomic discrimination (Plumb *et al*, 2005; Wilson *et al*, 2005). Lately, LC–MS has been shown to be a sensitive and quantitative method of analysis for identification of major bile acids in urine and plasma (Mims and Hercules, 2003, 2004). Historically, bile acid analysis has been hindered by difficulties in

separating many structurally similar compounds and isomers in a highly complex matrix. We have now developed and show here for the first time an enhanced bile-acid-targeted profiling method using UPLC–MS, which gives superior chromatographic resolution and sensitivity (Wilson *et al*, 2005; Plumb *et al*, 2006) and greatly aids the study of bile acid metabolism.

In the present study, the complex metabolic response of the host to perturbation of its enteric microbiota at the systems level by integration of metabolic data from many compartments was investigated. The aim of the study is to assess the effects of the induction of a nonadapted microflora in a murine model (human baby flora (HBF)) on the host metabolism by comparison with animals colonized with a natural gut microflora (conventional), the result of a long period of co-evolution. An additional group of germfree mice, naturally re-conventionalized, was used as a control to investigate the specific effects related to the re-establishment of a flora in previously germfree mice. Here, we have integrated the effects of modulation of the microbiome in mouse models on major bile acids co-metabolism through targeted metabolic profiling, and characterized the consequences of this intervention at the systems level through parallel untargeted metabolic profiling, multivariate and graph modeling. Here, we show a significant association of specific metabotypes and changes of the gut microbiome between mice colonized naturally with a conventional microflora or colonized with a defined microbial population derived from human host in a pathogen-free environment, that is, HBF. This study brings further evidence that gut microflora is adapted to each host and that gut microflora influences the host's systemic lipid metabolism and energy balance through modification of bile acid metabolism and eventually impacts on the host's health.

Table I Microbial species counts in mouse feces at the end of the experiment

Groups/ $\log_{10}$ CFU	Conventional (N=10)	Re-conventional (N=10)	HBF-*L. paracasei* (N=7)
Lactobacilli	6.4±1.5	5.9±2.5	7.1±0.4
Enterobacteria	6.5±1.0	7.8±0.7**	9.1±0.4***[a]
Bifidobacteria	7.0±1.2	7.8±1.4	7.5±0.7
Staphylococcus	4.8±0.7	4.7±1.0	5.8±0.4
C. perfringens	<2	<2	7.0±0.9***[a]
Bacteroides	8.3±0.4	9.1±0.6**	9.5±0.9***

$\log_{10}$ of CFU (colony-forming unit) given per gram of wet weight of feces. Data are presented as mean±s.d. The average values for the re-colonized group were compared to the conventional animals: *significant difference at 95% confidence level, **significant difference at 99% confidence level, ***significant difference at 99.9% confidence level.
[a]Significant difference at 99.9% confidence level was observed when compared to the re-conventionalized animals.

Results

Gut bacterial composition and fecal content of short-chain fatty acids

Microbiological profiles were used to assess the stage of bacterial development during re-conventionalization and colonization with an HBF. The terminal composition of the fecal microbiota is detailed in Table I. Using a two-tailed Mann–Whitney test, we showed that after 32 days of natural re-conventionalization, the mice have similar microbial composition in feces as conventional animals, although their levels of *Bacteroides* and *Enterobacteria* were higher (Table I). The HBF mice had markedly different gut microbiota characterized by an important population of *Clostridium* and higher levels of *Bacteroides* and *Enterobacteria* as those observed in re-conventionalized mice when compared to conventional mice (Table I).

The fecal content of individual animals was investigated using gas-chromatography–flame-ionization-detection (GC–FID) to identify and quantify some major bacterial short-chain fatty acids (SCFAs), namely acetate, propionate, isobutyrate, *n*-butyrate, *n*-valerate and isovalerate. Although lactate changes were expected, they were not in fact measured. The results presented in Table II are given in μmol/g of dry fecal content, and as mean±s.d. for each group of mice, and were assessed using a two-tailed Mann–Whitney test. The production of SCFAs by the gut microbiota of re-conventionalized mice was similar to that of conventional mice, except that the latter has higher levels of acetate. These SCFAs were found in lower concentrations and in different proportions in HBF mice (Table II). In particular, a higher proportion of propionate (24.5±4%) and a lower proportion of *n*-butyrate (4.2±3.4%) were observed in HBF mice (controls were 10.2±1.2 and 11.1±3.4%, respectively).

^{1}H NMR spectroscopy of mouse plasma, urine, liver and ileal flushes

Examples of typical ^{1}H NMR spectra of urine, ^{1}H CPMG NMR spectra of liver and plasma from an HBF mouse, and ^{1}H NMR spectra of ileal flushes from HBF and conventional mice are shown in Figure 2 and were assigned according to literature (Nicholson *et al*, 1995; Tugnoli *et al*, 2004; Wang *et al*, 2005), and confirmed by selected ^{1}H-^{1}H correlation spectroscopy

Table II Short-chain fatty acid content in the cecum from the different groups

SCFAs\microbiota	Acetate	Propionate	Isobutyrate	Butyrate	Isovalerate	Valerate
Conventional	179.1±43.5 (73.7±3.5)	24.4±5.3 (10.2±1.2)	3.1±0.5 (1.3±0.2)	27.1±11.7 (11.1±4.3)	4.7±1.3 (2±0.4)	4.2±1 (1.7±0.4)
Re-conventional	136.6±51.4* (67±4.2**)	26.5±6.4 (14.5±3.7***)	3.3±0.8 (1.7±0.4**)	27.5±13 (12.1±4.3)	4.6±1.2 (2.5±0.8)	4.5±1.2 (2.2±0.5*)
HBF-*L. paracasei*	34.4±9.9*** (65.9±3.1***)	12.8±4*** (24.5±4***)	0.6±0.1*** (1.2±0.3**)	1.9±0.9*** (4.2±3.4***)	1.7±0.9*** (3.3±1.4***)	0.4±0.1*** (0.9±0.5**)

Data are presented in μmol/g of dry feces and are presented as means±s.d. The relative composition in short-chain fatty acids in percentage of total content. The average values for the re-colonized group were compared to the conventional animals: *significant difference at 95% confidence level, **significant difference at 99% confidence level, ***significant difference at 99.9% confidence level.

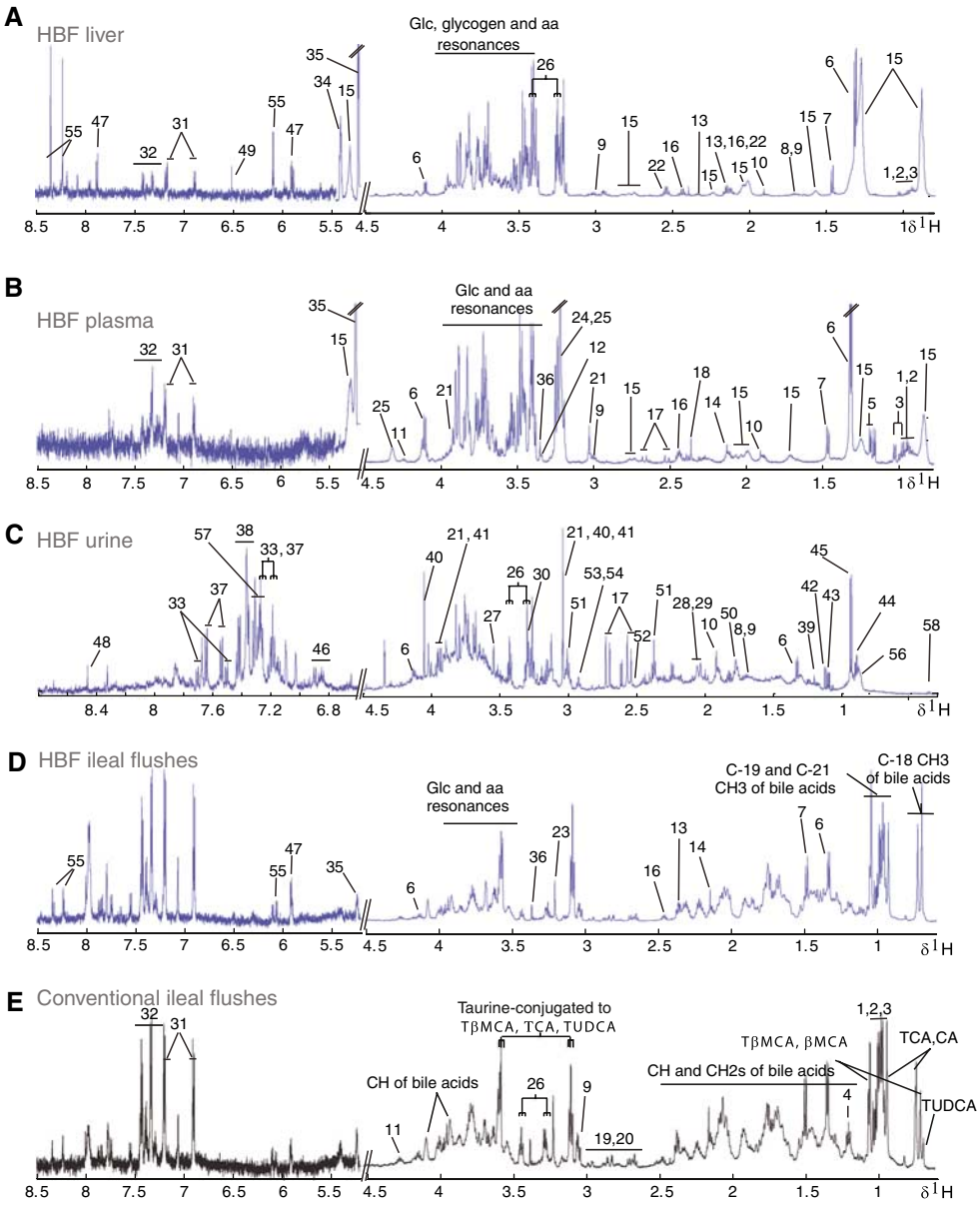

Figure 2 Typical 600 MHz ^{1}H NMR spectra. ^{1}H CPMG NMR spectra of plasma (**A**) and intact liver tissue (**B**), and ^{1}H NMR spectrum of urine (**C**) from an HBF mouse, and ^{1}H NMR spectra of ileal flushes from HBF (**D**) and conventional mice (**E**). The spectra of the urine and ileal flushes were magnified 6 and 10 times respectively in the aromatic region (δ 5.2–8.5) compared to the aliphatic region (δ 0.7–4.5). The liver regions δ 5.2–5.4 and 5.4–8.5 were magnified 4 and 8 times respectively. The plasma regions δ 5.2–5.4 and 5.4–8.5 were magnified 4 and 10 times respectively. Keys to the figures are given in Table III.

(COSY) (Hurd, 1990) and ^{1}H-^{1}H total correlation spectroscopy (TOCSY) (Bax and Davis, 1985) two-dimensional (2D) NMR experiments on single sample as well as selective statistical total correlation spectroscopy (STOCSY) (Cloarec *et al*, 2005a) experiments on multiple samples. In particular, NMR spectroscopy detects a wide range of amino acids, metabolism intermediates, organic acids, membrane components, saturated and unsaturated triglycerides and fatty acids, ketone bodies, *N*-acetyl and *O*-acetyl-glycoproteins (Table III). Indoleacetylglycine (IAG), phenylacetylglycine (PAG), trimethylamine (TMA), trimethylamine-*N*-oxide (TMAO) and dimethylglycine (DMG) were also identified in urine. Using NMR, five bile acid species were assigned unambiguously in ileal flushes, that is, β-muricholic (βMCA), tauro-β-muricholic (TβMCA), cholic (CA), taurocholic (TCA) and tauroursodeoxicholic (TUDCA) acids. ^{1}H NMR spectra of pure compound showed that the ^{1}H NMR chemical shifts of C-18, C-19 and C-21 methyl groups were characteristic for the determination of individual bile acid levels. However, this method is of limited use for probing complex mixtures and for differentiating conjugated from unconjugated forms of bile acids in such mixtures.

^{1}H NMR spectral complementary data sets from plasma, urine, liver tissue or ileal flushes were analyzed using orthogonal partial least squares discriminant models (O-PLS-DA) (Trygg and Wold, 2003) to maximize the discrimi-

Table III Table of assignment of the metabolites in plasma, liver, urine and ileal flushes

Key	Metabolites	Moieties	δ ^{1}H (p.p.m.) and multiplicity
1	Isoleucine	αCH, βCH, γCH_3, δCH_3	3.65(d), 1.95(m), 0.99(t), 1.02(d)
2	Leucine	αCH, βCH_2, δCH_3, δCH_3	3.72(t), 1.96(m), 0.91(d), 0.94(d)
3	Valine	αCH, βCH, γCH_3	3.6(d), 2.26(m), 0.98(d), 1.04(d)
4	Ethanol	CH_2, βCH_3	3.65(q), 1.18(t)
5	3-D-hydroxybutyrate	CH, CH_2, γCH_3, CH_2	4.16(dt), 2.41(dd), 1.20(d), 2.31(dd)
6	Lactate	αCH, βCH_3	4.11(q), 1.32(d)
7	Alanine	αCH, βCH_3	3.77(q), 1.47(d)
8	Arginine	αCH, βCH_2, γCH_2, δCH_2	3.76(t), 1.89(m), 1.63(m), 3.23(t)
9	Lysine	αCH, βCH_2, γCH_2, δCH_2, εCH_2	3.77(t), 1.89(m), 1.72(m), 1.47(m), 3.01(t)
10	Acetate	CH_3	1.91(s)
11	Threonine	αCH, βCH_2, γCH_3	3.59(d), 4.25(m), 1.32(d)
12	Proline	αCH, βCH_2, γCH_2, δCH_2	4.11(t), 2.02(m)–2.33(m), 2.00(m), 3.34(t)
13	Glutamate	αCH, βCH_2, γCH_2	3.75(m), 2.08(m), 2.34(m)
14	Methionine	αCH, βCH_2, γCH_2, δCH_3	3.78(m), 2.14(m), 2.6(dd), 2.13(s)
15	Lipids	CH_3, (CH_2)n, CH_2-C=C, CH_2-C=O, =C-CH_2-C=, -CH=CH-	0.89(m), 1.27(m), 2.0 (m), 2.3(m), 2.78(m), 5.3(m)
16	Glutamine	αCH, βCH_2, γCH_2	3.77(m), 2.15(m), 2.44(m)
17	Citrate	CH_2(2), CH_2(1)	2.55(d), 2.65(d)
18	Pyruvate	CH_3	2.41(s)
19	Aspartic acid	αCH, βCH_2	3.89(m), 2.68(m), 2.82(m)
20	Asparagine	αCH, βCH_2	3.90(m), 2.86(m) 2.94(m)
21	Creatine	N-CH_3, CH_2	3.03(s), 3.92(s)
22	Glutathione	CH_2, CH_2, S-CH_2, N-CH, CH	2.17(m), 2.55(m), 2.95(m), 3.83(m), 4.56(m),
23	Choline	N-(CH_3)3, OCH_2, NCH_2	3.2(s), 4.05(t), 3.51(t)
24	Phosphorylcholine	$N(CH_3)$3, OCH_2, NCH_2	3.22(s), 4.21(t), 3.61(t)
25	GPC	N-(CH_3)3, OCH_2, NCH_2	3.22(s), 4.32(t), 3.68(t)
26	Taurine	N-CH_2, S-CH_2	3.26(t), 3.40(t)
27	Glycine	CH_2	3.55(s)
28	*N*-acetyl-glycoproteins (Nac)	CH_3	2.04(s)
29	*O*-acetyl-glycoproteins	CH_3	2.08(s)
30	Trimethylamine-*N*-oxide (TMAO)	CH_3	3.26(s)
31	Tyrosine	CH, CH	7.16(dd), 6.87(dd)
32	Phenylalanine	2,6-CH, 3,5-CH, 4-CH	7.40(m), 7.33(m), 7.35(m)
33	Tryptamine	4-CH, 7-CH, 2-CH, 6-CH, 5-CH, CH_2, CH_2	7.70(d), 7.52(d), 7.34(s) 7.29(t), 7.21(t), 3.35(t), 3.18(t)
34	Glycogen	Ring protons, CH	3.35–4.0(m), 5.38–5.45(m)
35	α-Glucose	1-CH	5.24(d)
36	Scyllo-inositol	OH	3.34(s)
37	Indoleacetyl-glycine (IAG)	4-CH, 7-CH, 2-CH, 5-CH, 6-CH, CH_2, CH_2	7.64(d), 7.55(d), 7.35(s) 7.28(t), 7.19(t), 3.82(s), 3.73(s)
38	Phenylacetyl-glycine (PAG)	2,6-CH, 3,5-CH, 7-CH, 10-CH	7.43(m), 7.37(m), 3.75(d), 3.68(s)
39	3-Hydroxy-isovalerate	CH_3	1.21(s)
40	Creatinine	CH_3, CH_2	3.06(s), 4.06(s)
41	Phosphocreatine	CH_3, CH_2	3.05(s), 3.95(s)
42	Isobutyrate	CH_3, CH	1.11(d), 3.02(m)
43	α-Ketoisovalerate	CH_3, CH	1.13(d), 3.02(m)
44	Butyrate	CH_3, CH_2, CH_2	0.90(t), 2.16(t), 1.56(m)
45	α-Keto-isocaproate	CH_3, CH, CH_2	0.94(d), 2.10(m), 2.61(d)
46	Kynurenine	CH, CH, CH, CH, CH, CH	4.16(t), 3.72(d), 7,89(d), 6.82(t), 7.43(t), 6.89(d)
47	Uridine	CH, CH, CH, CH, CH, CH, CH_2, CH_2	7.87(d), 5.92(d), 5.9(s), 4.36(t), 4.24(t), 4.14(q), 3.92(dd), 3.81(dd)
48	Formate	CH	8.45(s)
49	Fumarate	CH	6.53(s)
50	Citrulline	CH, CH_2, CH_2, CH_2	3.76(t), 3.15(q), 1.88(m), 1.52(m)
51	2-Oxoglutarate	CH_2, CH_2	3.01(t), 2.45(t)
52	β-Alanine	CH_2, CH_2	3.19(t), 2.56(t)
53	Dimethylglycine (DMG)	CH_2	2.93(s)
54	Trimethylamine (TMA)	CH_3	2.91(s)
55	Inosine	2-CH, 8-CH, 2′-CH, 4′-CH, 5′-CH, CH_2, CH_2	8.34(s), 8.24(s), 6.1(d), 4.44(t), 4.28(q), 3.92(dd), 3.85(dd)
56	Putative glycolipid (U1)	CH_3, CH_2, —	0.89(m), 1.27(m), 1.56(m), 1.68(m), 2.15(m), 2.25(m), 3.10(m), 3.55(m), 3.60(m)
57	*p*-Toluyl derivative (U2)	CH_3, CH_2, CH_2, CH_2	2.38(s), 7.31(d), 7.26(d), 5.42(m)
58	Unknown (U3)	—	0.37(t), 0.66(m), 0.74(m), 0.90(m), 1.15(m), 1.35(m), 2.24(m)
59	Unknown (U4)	—	3.49(s), 1.14(d)
60	Glycerol	C2-H, CH_2, CH_2	3.91(m), 3.64(m), 3.56(m)

s, singlet; d, doublet; t, triplet; q, quartet; m, multiplet; dd, doublet of doublet; dt, doublet of triplet.

nation of experimental groups and focus on metabolic variations explained to gut flora changes (Figure 3). The characteristics of the models generated are summarized in Table IV. O-PLS-DA revealed significant variations in the metabolic profiles from plasma, liver and urine between conventional and re-conventionalized animals (Table IV). Re-conventionalized

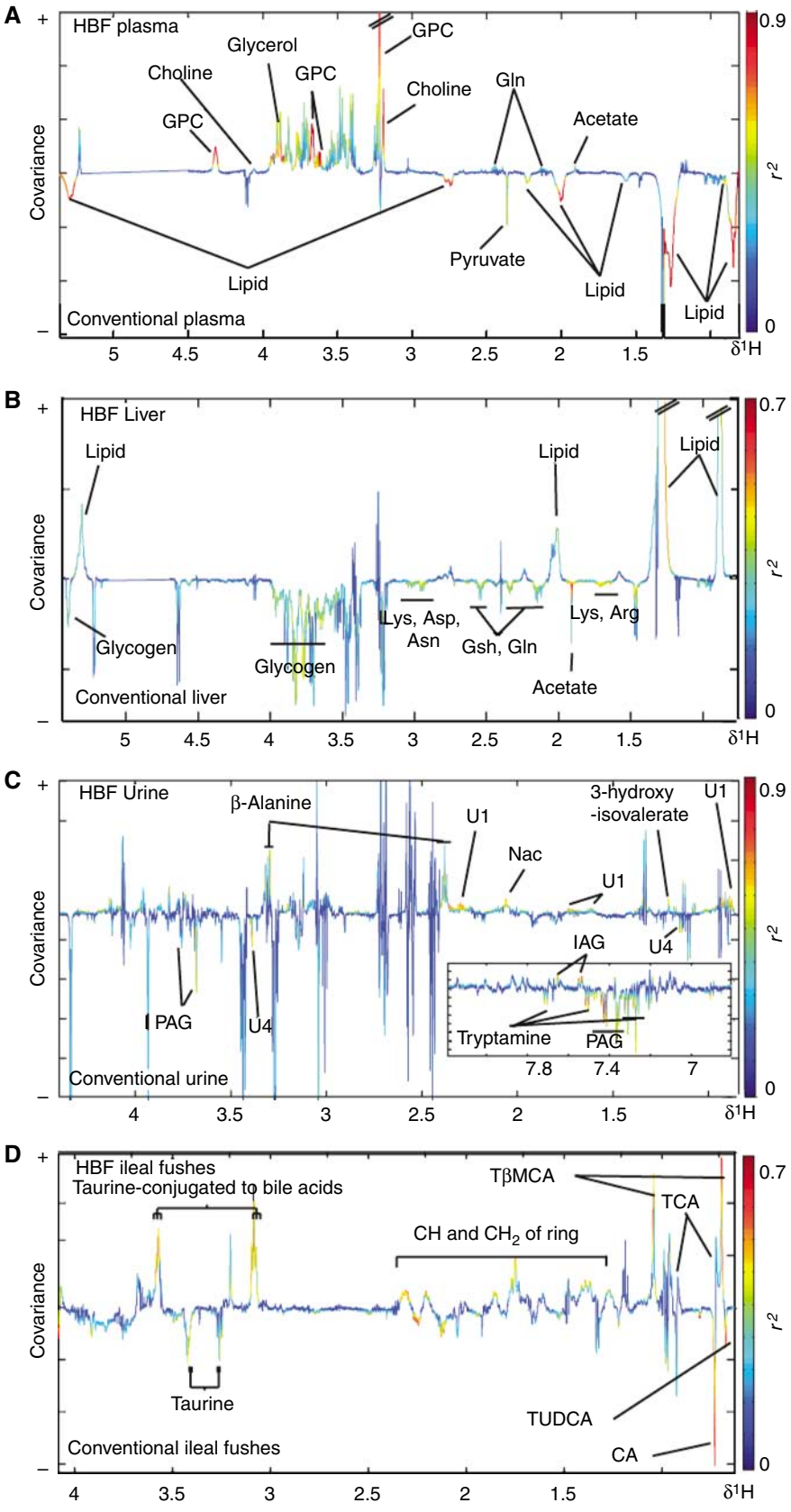

Table IV O-PLS-DA model summary for discriminating NMR spectra of plasma, urine, liver and ileal flushes

Discrimination analyzed/sample	Conventional versus re-conventionalized	Conventional versus HBF
Plasma	Q^2Y=29%, R^2X=23%	Q^2Y=70%, R^2X=28%
Urine	Q^2Y=40%, R^2X=37%	Q^2Y=75%, R^2X=44%
Liver	Q^2Y=42%, R^2X=54%	Q^2Y=46%, R^2X=54%
Ileal flushes	$Q^2Y < 0$	Q^2Y=35%, R^2X=84%

O-PLS models were generated with (1) predictive component and (2) orthogonal components to discriminate between two groups of mice. The R^2X value shows how much of the variation in the data set X is explained by the model. The Q^2Y value represents the predictability of the models and relates to its statistical validity. A negative value indicates that differences between groups are statistically nonsignificant.

mice had higher levels of plasma GPC and choline, lower urinary concentrations of guanidinoacetate and lower levels of liver glycogen (data not shown).

Significant and predictive discrimination of plasma, liver, urine and ileal flushes between conventional and HBF mice was achieved using O-PLS-DA, as denoted by high Q^2Y values (Table IV). The corresponding coefficient plots show the key metabolites in plasma, liver, urine and ileal flushes that contribute to the separation (Figure 3). Decreases in levels of lipoproteins and pyruvate, and increased levels of GPC, choline, acetate and glutamine were observed in the plasma of HBF mice when compared to conventional animals (Figure 3A and Supplementary Figure 1). The liver of HBF mice also showed higher levels of triglycerides and lower concentrations of glycogen, lysine, arginine, asparagine, aspartate, glutamine and glutathione (Figure 3B and Supplementary Figure 1). Urinary profiles of HBF mice showed lower levels of PAG, tryptamine and an unknown metabolite (U1), and higher levels of β-alanine, 3-hydroxy-isovalerate, *N*-acetyl signals from glycoproteins and a putative glycolipid as discussed earlier (Figure 3C). Differences in the ileal flushes were also characterized with higher levels of TβMCA and lower levels of CA and TUDCA (Figure 3D).

UPLC–MS analysis and ileal content in bile acids

To complement the bile acid profiling achieved by NMR, we also analyzed ileal flushes using UPLC–MS. Typical negative ion chromatograms for the bile acids detected in the ileal flush of a conventional mouse are shown in Figure 4. A total of 14 bile acids were identified by comparison with a series of 22 bile acid standards. Three additional bile acid components, identified as U1 (m/z=453.2, RT=2.70), U2 (m/z=437.2, RT=4.44) and U3 (m/z=491.2, RT=1.53), were also observed. Unconjugated muricholic and cholic acids with mass to charge ratio of m/z=408.2 were detected at m/z=453.2 due to the formation of a formate adduct (45 Da).

The relative bile acid compositions in ileal flushes from the different groups are given in Table V, and are shown as mean ± s.d. of the percentage of the total bile acid content. UPLC–MS analysis showed that conventional and re-conventionalized mice had specific bile acid profiles—14 bile acids were identified, the most abundant species being CA, TCA, TβMCA and TUDCA. HBF animals showed lower diversity in their bile acid composition, predominantly containing TβMCA and TCA as well as CA, αMCA, βMCA, TCDCA, TUDCA and putative unknown bile acid U3.

A comparison of concentrations of bile acids obtained from HBF re-colonized mice with those from conventional mice using an O-PLS-DA strategy revealed that conventional mice showed lower amounts of taurine conjugates such as TβMCA and TCA, and a higher amount of CA, which is in agreement with the observations obtained by ^{1}H NMR spectroscopy (Figure 5A). A weak discrimination was also obtained between conventional and re-conventionalized animals (Figure 5B), with the latter showing lower levels of CDCA and GCA, and higher concentrations of TβMCA.

Effect of major bile acids on tissue-specific metabolic profiles

The effect of TCA and CA on the enterohepatic recirculation was assessed by OPLS regression, using the NMR-based metabolic profiles from intact liver tissues and ileal luminal content as **X** input and CA (or TCA) levels obtained by UPLC–MS as **Y** (Figure 6). The ^{1}H NMR metabolic profiles obtained from ileal flushes (Figure 6B and D) show a marked anticorrelation between TCA and CA, these two major bile acids operating as 'anchor' metabolites. There is a positive correlation between conjugated taurine and taurine-conjugated bile acids, that is, TCA and TβMCA. This cluster of conjugated species is anticorrelated to free species, that is, CA and free taurine, consistent with a bacterial deconjugation of bile acids in the ileum. In the liver (Figure 6A and C), the situation is reversed, with TCA (CA) being correlated (anticorrelated) with free taurine, highlighting the fact that the conjugation process is restricted by the available amount of taurine (substrate).

Integration of correlations between bile acids and fecal flora

A novel correlative analysis was performed to investigate the cross-compartment connections between fecal flora and bile acids in the intestinal lumen. Bipartite graphs were used to visualize correlations (above a given cutoff) between fecal bacteria and bile acids (see Materials and methods and Figure 7). Conventional and HBF mice show very different bile acid/fecal flora correlation networks (Figure 7A and B).

Figure 3 O-PLS-DA coefficient plots derived from ^{1}H NMR spectra. O-PLS-DA coefficient plots derived from ^{1}H NMR CPMG spectra of plasma (**A**), ^{1}H MAS NMR CPMG spectra of liver (**B**) and ^{1}H NMR spectra of urine (**C**) and ileal flushes (**D**) indicating discrimination between conventional (negative) and HBF-colonized mice (positive). The O-PLS-DA coefficient plots are presented using a back-scaling transformation, as described previously (Cloarec *et al*, 2005b), which allows each variable to be plotted with a color code that relates to the significance of class discrimination as calculated from the correlation matrix. Arg, arginine; Asp, aspartate; Asn, asparagine; CA, cholic acid; Gln, glutamine; Gsh, glutathione; GPC, glycerophosphorylcholine; IAG, indoleacetylglycine; Lys, lysine; Nac, *N*-acetyl-glycoproteins; PAG, phenylacetylglycine; TCA, taurocholic acid; TβMCA, Tauro β muricholic acid; TUDCA, tauroursodeoxycholic acid.

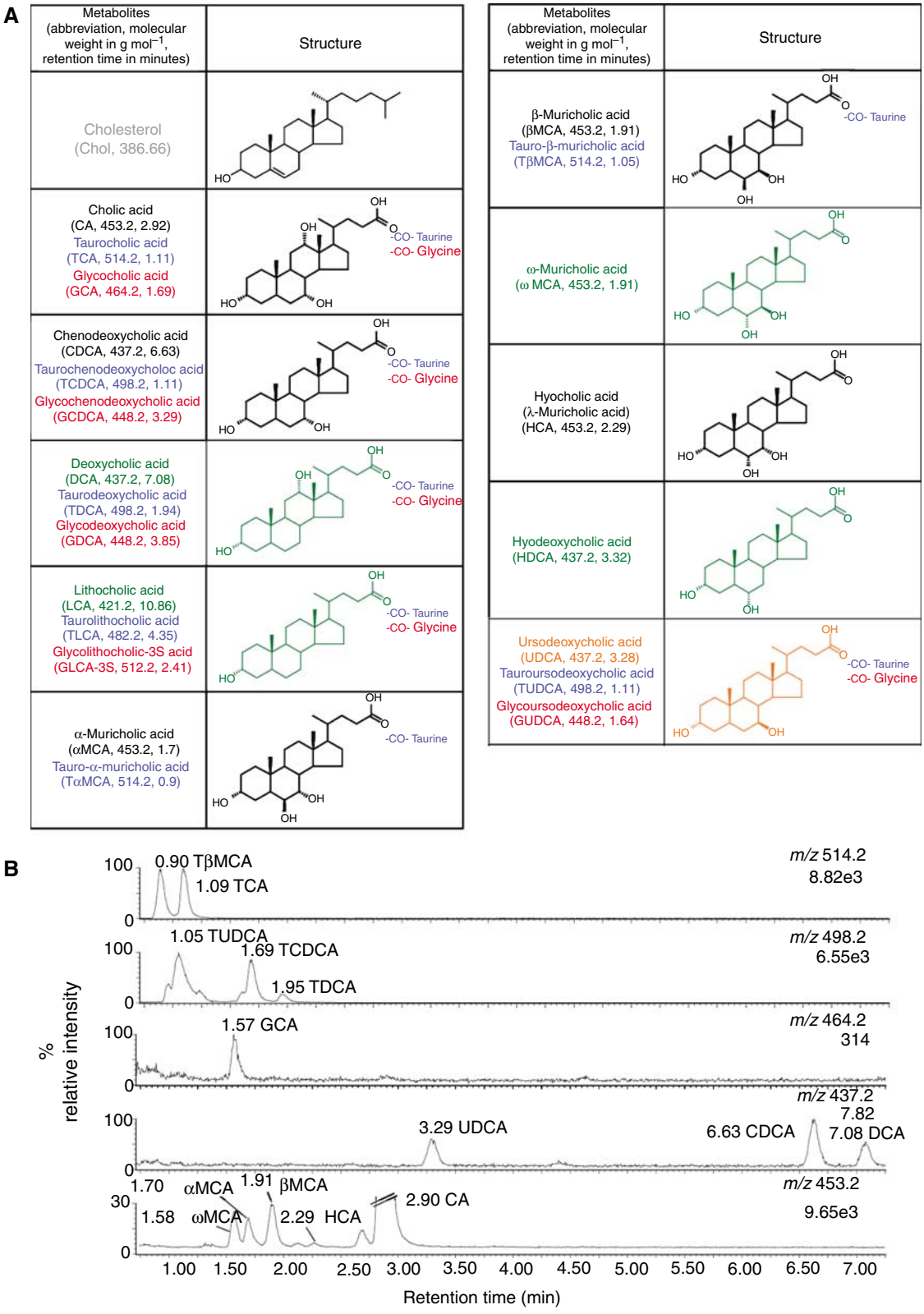

Figure 4 Structural and functional study of bile acids. Structures of bile acids and cholesterol (**A**), as characterized in this study. Color denotes family of bile acids, that is, primary (black), secondary (green) and tertiary (orange). Conjugation with taurine and glycine is colored in blue and red respectively. Key intermediates in the pathway are colored in gray. Typical negative ion mass chromatograms from the UPLC–MS analysis (**B**) for the ions detected at the given *m/z* for the ileal flush from a conventional mouse with sample injections of 10 μl (1 μl for *m/z*=514.2). Numbers under the *m/z* ratios are the total ion counts for that chromatogram.

Network statistics given for several correlation cutoffs (Figure 7C) reveal that microbiome/metabolome bipartite graphs from HBF mice show in general lower complexity than conventional mice. In particular, for $|r| > 0.5$, we observed that in the conventional flora network of degree 9, the most connected bacteria are *Lactobacilli* (correlated to nine different bile acids, Figure 7A). HBF mice are supplemented with one *Lactobacillus* strain (*Lactobacillus paracasei*) for which only one functional correlation is significant, whereas the most connected bacteria are *Enterobacteria* (*Escherichia coli*) (correlated to three bile acids; Figure 7B).

Table V Bile acids composition in gut flushes for the different microbiota

Microbiota/bile acids	Conventional	Re-conventional	HBF
DCA	0.7±0.5	1±1	ND
CDCA	0.5±0.1	0.2±0.1	ND
UDCA	0.5±0.2	0.7±0.6	ND
CA	17.7±6.7	12.7±9.1	0.4±0.5
ωMCA	0.8±1	0.7±0.5	ND
αMCA	0.9±0.7	0.6±0.5	0.3±0.2
βMCA	1.6±1	1.9±1.4	0.9±0.7
HCA	0.1±0.1	0.1±0.1	ND
GCA	0.3±0.1	0.1±0.1	ND
TDCA	0.7±0.4	0.6±0.6	ND
TCDCA	1.9±1.3	1.1±0.6	3.3±1
TUDCA	5.5±2.3	4.7±0.8	6.6±1.4
TβMCA	42.6±4.2	52.4±7.6	49.6±4.8
TCA	23.2±13.3	22±19.4	38±3.4
Ratio TCA:CA	1.4	1.7	118.8
Ratio TβMCA:βMCA	24.0	27.7	52.0

NB: Relative composition in bile acids given in percentage of total bile acid content. Species not detected with UPLC-MS experiment are shown as ND.

Discussion

We have investigated the host's metabolic response to perturbation of its enteric microbiota at the systems level, using multiple compartment information deriving from 'state-of-the-art' metabolic profiling technologies combined with novel data analysis methods. A significant association between changes of the gut microbiome and specific metabotypes (obtained from urine, plasma, intact liver tissue and ileal flush) in mice was shown. This study brings further evidence that gut microbiota modulates the host systemic lipid metabolism through (i) modification of bile acid metabolic patterns, impacting directly on (ii) emulsification and absorption properties of bile acids and then indirectly on (iii) storage of fatty acids in liver and (iv) lipoperoxidation through bile acid signaling properties, as detailed below (Figure 8).

Modulation of bile acid conjugative patterns by gut microbiota

The various properties of bile acids provide a complex signaling system in which the gut microflora finely interacts with the host's metabolism. Previous analyses in rodents (Floch, 2002) reported that the liver secretes almost 100% tauro-conjugated bile acids in the bile (typically 60% TβMCA

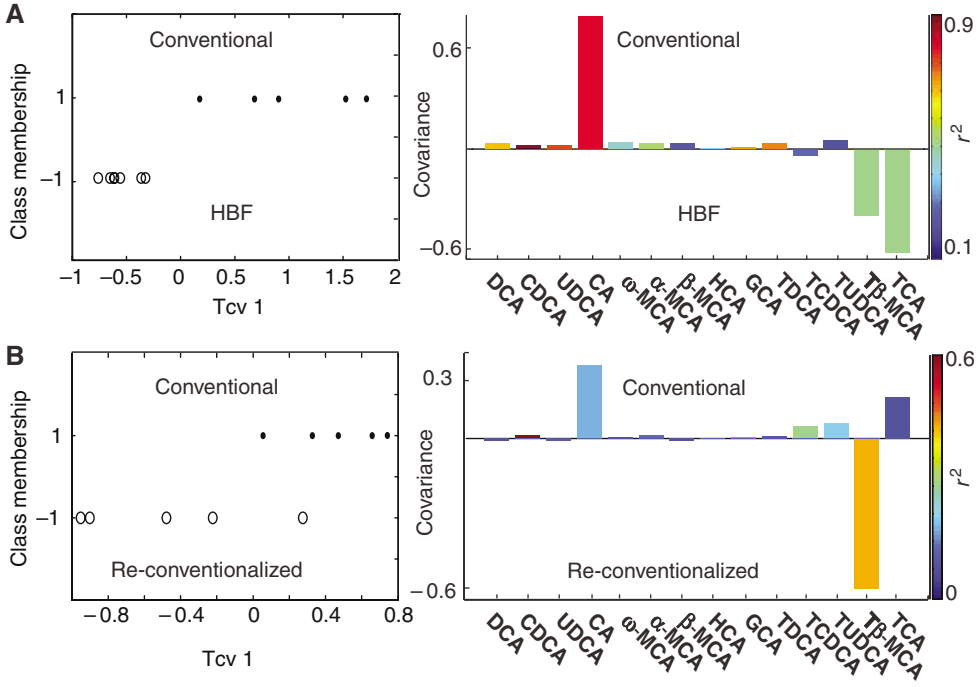

Figure 5 O-PLS-DA coefficient plots derived from the UPLC–MS bile acid composition. O-PLS-DA coefficient plots derived from the bile acid composition obtained by UPLC–MS analysis of ileal flushes, indicating discrimination between conventional (positive) and HBF colonized mice (negative) (**A**), and partial discrimination between conventional (positive) and re-conventionalized mice (negative) (**B**). The color code corresponds to the correlation coefficients of the variables. One predictive and one orthogonal components were calculated, and the respective (Q^2Y, R^2X) are (89.1%, 80%) and (51.4%, 62%). The O-PLS-DA coefficient plots are presented using a back-scaling transformation, as described previously (Cloarec *et al*, 2005b), which allows each variable to be plotted with a color code that relates to the significance of class discrimination as calculated from the correlation matrix.

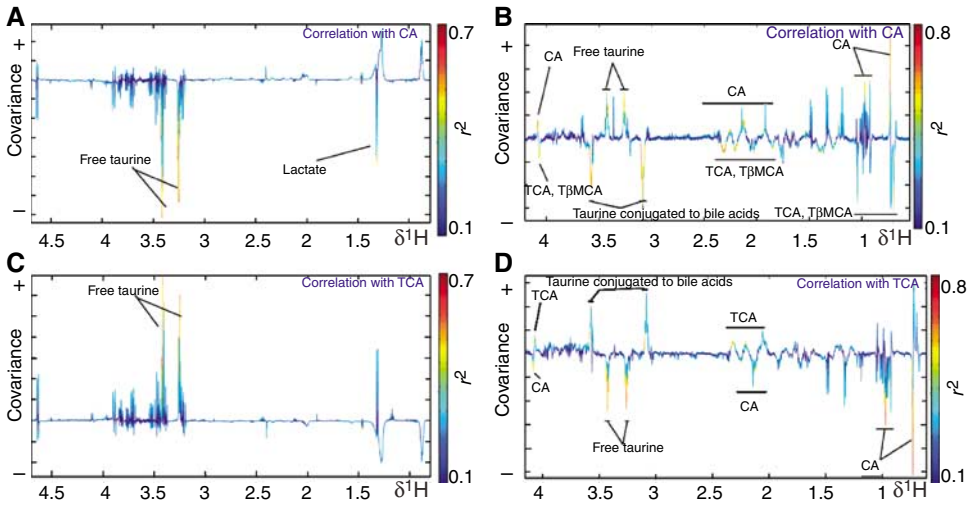

Figure 6 Effect of major bile acids on organ-specific metabolic profiles. O-PLS coefficient plots describing correlation between ^{1}H NMR spectra of ^{1}H MAS NMR CPMG spectra of liver (**A, C**) and ileal flushes (**B, D**) and ileal concentrations of cholic acid (A, B) and taurocholic acid (C, D), as measured using UPLC–MS. The O-PLS coefficients plots are presented using a back-scaling transformation, as described previously (Cloarec *et al*, 2005b), which allows each variable to be plotted with a color code that relates to the significance of correlation as calculated from the correlation matrix. One predictive and two orthogonal components were calculated; the respective (Q^2Y, R^2X) are (55%, 39%), (47%, 37%), (36%, 44%) and (21%, 41%). CA, cholic acid; TCA, taurocholic acid.

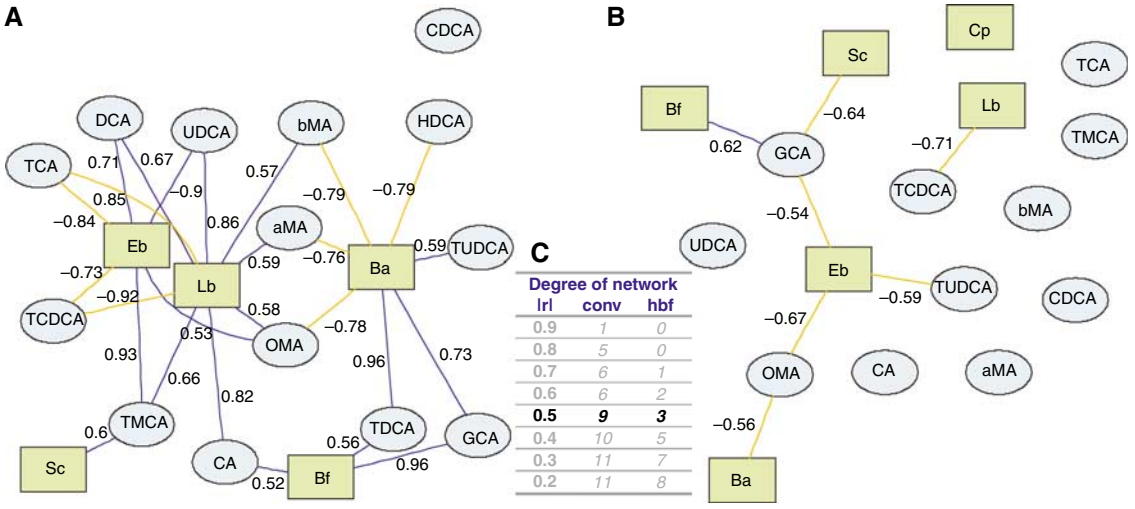

Figure 7 Integration of bile acid and fecal flora correlations. The bipartite graphs were derived from correlations between fecal flora and bile acids in each group: conventional (**A**) or HBF (**B**). $G=(N,E)$ specifies a graph G with N denoting the node set (bile acids) and E the edge set (correlation between bile acids, above a defined cutoff, that is, $|r| > 0.5$), which was defined using network degree statistics (**C**). Bile acids and fecal bacteria correspond to blue ellipse nodes and green rectangle nodes respectively. Edges are coded according to correlation value: positive and negative correlations are respectively displayed in blue and orange. aMA, α-muricholic acid; Ba, *Bacteroides*; Bf, *Bifidobacteria*; bMA, β-muricholic acid; CA, cholic acid; CDCA, chenodeoxycholic acid; Cp, *Clostridium perfringens*; DCA, deoxycholic acid; Eb, *Enterobacteria*; GCA, glycocholic acid; HCA, hyocholic acid; Lb, *Lactobacillus*; OMA, ω-muricholic acid; Sc, *Staphylococcus*; TCA, taurocholic acid; TCDCA, taurochenodeoxycholic acid; TDCA, taurodeoxycholic acid; TMCA, tauro-β-muricholic acid; TUDCA, tauroursocholic acid; UDCA, ursocholic acid.

and 40% TCA). In our study on conventional and re-conventionalized mice**,** primary, secondary and tertiary bile acids are observed as unconjugated, tauro- and glyco-conjugated species ileal flushes (Table V). These observations illustrate the ability of 'healthy and normal' gut microbiota (Hooper and Gordon, 2001) to deconjugate bile acids and modify them as detailed in Figure 1 and previously (De Smet *et al*, 1998; Ridlon *et al*, 2006). The bacterial composition of HBF implemented in a murine gastrointestinal ecosystem is similar to that found in human gastrointestinal tracts (Backhed *et al*, 2004; Kibe *et al*, 2005). It is also significantly different from conventional microbiota in terms of bacterial species and relative composition, that is, higher levels of *Enterobacteria* and *Bacteroides* (Table I). Our results show that significant variations in microbial populations lead to modification of bile acid symbiotic metabolism in the ileal lumen (Figures 3 and 5; Table V). Furthermore, similar to HBF mice, re-conventionalized mice also show elevated levels of *Enterobacteria* and *Bacteroides* and high concentrations of TβMCA when compared to conventional mice (Figure 5). The deconjugation of

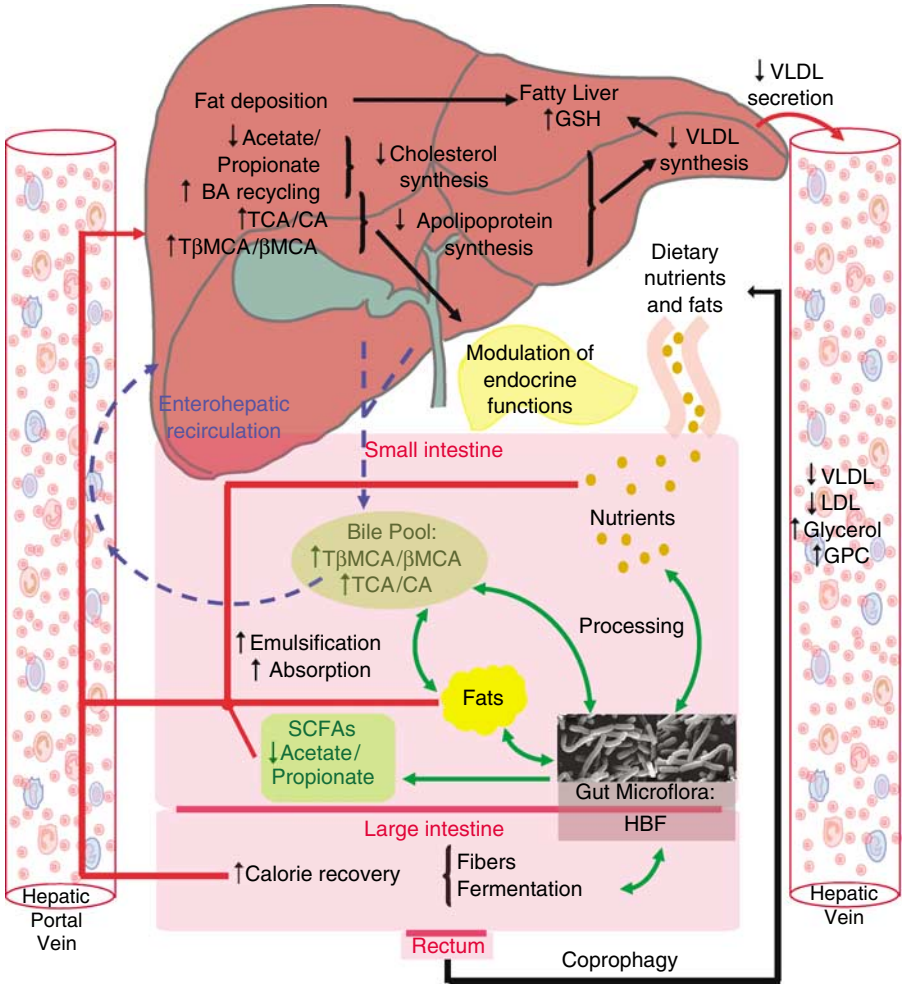

Figure 8 Microbe–mammalian metabolic interactions related to bile acid and lipid metabolism. The bacterial reprocessing of the bile acid pool and regulation of bile acid metabolism by bacterial SCFAs affect significantly the enterohepatic recirculation and the systemic lipid metabolism, that is, emulsification, absorption, transport of dietary fats. The gut bacterial-induced regulation of enterohepatic recirculation also led to a physiological regulation of oxidative stress (glutathione), reprocessing of fatty acids (deposition, apoprotein and VLDL synthesis) and VLDL secretion from the liver, which result in controlling the influx and efflux of fatty acids in the liver. BA, bile acids; CA, cholic acid; GPC, glycerophosphorylcholine; GSH, glutathione; HBF, human baby flora; LDL, low-density Lipoproteins; βMCA, β-muricholic acid; SCFAs, short-chain fatty acids; TβMCA, tauro-β-muricholic acid; TCA, taurocholic acid; VLDL, very low-density lipoproteins.

bile acids involves the activity of bile salt hydrolase, which is synthesized in significant amounts by *Lactobacillus* and *Bifidobacteria* (De Smet *et al*, 1998). Alltogether, these observations suggest that the balance between *Lactobacillus* and *Bifidobacteria* and *Enterobacteria*, *Bacteroides* might be essential in the deconjugation of TβMCA.

To investigate transgenomic metabolic interactions, we show for the first time the use of bipartite graphs to display correlation patterns between fecal flora and bile acids (Figure 7). These graphs show the fine relationship between specific gut microbial population modulation and bile acid co-metabolism. For instance, the elevated concentrations of TβMCA in HBF mice correspond to a relative inability of HBF to deconjugate murine bile acids (Sacquet *et al*, 1984) and to transform further TβMCA into derivatized bile acids, such as ùMCA (Sacquet *et al*, 1979) or HCA (Eyssen *et al*, 1983) (Figure 1 and Table V). The overwhelming contrast between the simplicity of HBF mice and the complexity of conventional mice bipartite networks (Figure 7) highlights the contrast between the restrained abilities of the few bacterial strains composing HBF to transform bile acids, on the one hand, and the metabolic flexibility of conventional mice, on the other hand, whereby the conventional murine bacterial strains communicate with each other and disperse their metabolic functions to synthesize additional bile acids (DCA, CDCA, UDCA, ωMCA, HCA, GCA, TDCA). In this regard, the synthesis of ωMCA appears as a good example as it can only be achieved by specific bacterial strains (Sacquet *et al*, 1979) or through bacterial cooperation (Eyssen *et al*, 1983). In this regard, this lower complexity of the HBF bipartite network suggests lower metabolic flexibility and robustness.

The potential role of microbiome in fat emulsification and absorption

We observe a shift in the bile acid pattern towards tauro-conjugates in HBF, which can be explained by a lower deconjugation activity from the microbiota. Bile acids are

amphiphilic (hydrophobic and hydrophilic) compounds and conjugation modifies their hydrophobic/hydrophilic balance, which directly relates to lipid emulsification and eventually absorption (Armstrong and Carey, 1982; Heuman, 1989; Heuman *et al*, 1989). Tauro-conjugation of bile acids reduces the hydrophobic/hydrophilic ratio and increases their solubility and lipid emulsification. On the contrary, deconjugated bile acids are less effective in emulsification of dietary lipids and micelle formation (Armstrong and Carey, 1982; Heuman, 1989; Heuman *et al*, 1989; Narushima *et al*, 2000; Tannock, 2004). Here, we show that HBF mice have lower levels of CA and higher levels of TCA and TβMCA (Figures 3 and 5), with ratios of TCA:CA of 118.8 and TβMCA:βMCA of 52, whereas conventional mice showed ratios of TCA:CA of 1.4 and TβMCA:βMCA of 24 (Table V). These biochemical changes towards increasing lipid emulsion efficiency of the bile acid mixture (Staggers *et al*, 1982; Watkins, 1985) were also shown to modify the hepatic phase II taurine conjugation activity as described by the strong correlation between taurine concentration in the liver and ileal bile acid composition (Figure 6). This data integration clearly shows two opposite biological mechanisms: the tauro-conjugation process of CA into TCA in the liver, which is counterbalanced by a bacteria-mediated deconjugation process in the intestinal tract (ileum). Moreover, HBF mice show higher urinary excretion of β-alanine, which is a competitive inhibitor of taurine uptake in kidney and liver as it shares the same transporter (Bollard *et al*, 2005). The differences in β-alanine elimination also illustrate the different requirements of taurine in the metabolism of bile acids, which is consistent with higher demands in conventional animals for conjugation of bile salts. Our observations suggest increased hydrophilicity of the bile acid pool in HBF and re-conventionalized mice, which would lead to higher intestinal absorption of dietary lipids and higher enterohepatic recycling of bile acid pool when compared to conventional animals. Recent findings support our results with suggestion of the essential microbial role in affecting bile acid-controlled signaling pathways involved in energy and lipid metabolism (Houten *et al*, 2006; Watanabe *et al*, 2006). In particular, endogenous bile acids and derivates such as UDCA and TUDCA were shown to be chemical chaperones (osmolytes) with antidiabetic properties (Ozcan *et al*, 2006). Hence, the perturbation of the microbiota by modifying bile acid metabolism may ultimately affect the nutritional and wider health status of the host.

The gut microbiota modulate lipid metabolism in the host

The essential role of gut microbiota on serum lipid levels in humans has gained interest recently, in relation to the possible etiology of cardiovascular diseases (Pereira and Gibson, 2002). For instance, cholesterol-lowering effects were reported for *Lactobacillus* and *Bifidobacteria,* as well as protection against VLDL and LDL oxidation (Terahara *et al*, 2000; Xiao *et al*, 2003). These observations are consistent with previous findings that the microbiota promote storage of triglycerides in adipocytes via indirect modulation of cellular fatty acids uptake, secretion of apolipoproteins and adipocyte triglyceride accumulation (Backhed *et al*, 2004; Dumas *et al*, 2006). Lin *et al* (1996a, b) and Watanabe *et al* (2004) demonstrated that an increase in the intracellular bile acids concentration (in particular TCA) and decrease in hepatic bile acid synthesis inhibit the synthesis and secretion of VLDL-associated triglycerides from hepatocytes as well as the secretion of the apolipoprotein associated with transport of VLDL, namely apoB-100. These previous results indicate that bile acids might play a physiological role in regulating VLDL production by the liver, the enterohepatic circulation acting as a feedback loop. This provides a mechanistic model in which the symbiotic microbiota can modulate the host's lipid metabolism. The gut bacterial–mammalian metabolic interactions related to bile acid and lipid metabolism are summarized in Figure 8.

A microflora nonadapted to mice modulates the physiology of the host towards a pre-pathologic state

In the present study, mice re-colonized with HBF show decreased plasma lipoproteins concentration (mainly VLDL and LDL), increased glycerol, GPC and choline in plasma and increased hepatic triglyceride concentrations (Figure 3). Our results suggest that the higher enterohepatic recycling of TCA and TβMCA associated with higher intestinal absorption of dietary lipids in HBF mice leads to reduced synthesis and secretion of VLDL-associated triglycerides, and consequently accumulation of lipids in the liver and reduction of VLDL and LDL concentrations in plasma.

Such findings have to be interpreted simultaneously with lower concentrations of glutathione observed in the liver from HBF mice (Figure 3). Glutathione plays important roles in nutrient metabolism and antioxidant defense: depletion in glutathione contributes to oxidative stress, involved in the pathogenesis of several diseases, including cancer, liver disease, heart attack and diabetes (Wu *et al*, 2004). Previous observations reported reduced glutathione levels in the liver of rats fed with cholesterol plus cholic acid (Clarke *et al*, 1976; Girard *et al*, 2005), which is consistent with the observed higher intestinal absorption of dietary lipids and enterohepatic recycling of bile acid pool in HBF mice. Reprocessing of fatty acids and subsequent generation of radical oxidative species result in higher oxidative stress, this situation leading to peroxidation of hepatic lipids and eventually liver disease (Wu *et al*, 2004). Such glutathione depletion can be reached either by nutritional deficiency or by increased glutathione peroxidase and glutathione reductase activities in tissues. High oxidative stress denotes an increased lipoperoxidation risk (Figure 8). Altogether, our observations suggest that HBF is not a sustainable flora for mice, which might result in impaired liver functions.

In conclusion, both systemic and tissue-specific metabolic changes across a wide range of metabolic pathways and metabolite classes indicate the deep extent of host–microbiota co-metabolic interactions. This work strongly supports the idea that several complex metabolic disease traits can be influenced by the gut microbiota.

In this study, we have shown that re-conventionalization of mice normalizes their metabolism towards a healthy physiology. This metabolic convergence strikingly contrasts with our observations in the HBF model. We report that HBF is not a

sustainable flora for mice, which modifies the physiology of the murine host towards a pre-pathologic state. Whereas re-conventionalized mice evolve to normal gut flora from an ecological point of view, HBF supplementation maintains the gut tract and the liver out of a sustainable mouse ecological equilibrium, as denoted by higher numbers of *Clostridium perfringens* (Table I). The metabolic consequences for the host show an increase in lipid accumulation in liver (despite a decrease in lipoprotein sub-fractions in blood) associated to a higher lipoperoxidation risk. We also observed the critical involvement of the microbiome in supplying host calorific requirement via caloric recovery through fibers fermentation. In this case, gut bacteria exert modulation over the host metabolism via reprocessing of signaling molecules, that is, bile acids, that might be involved in common metabolic diseases such as obesity or type II diabetes (Houten *et al*, 2006; Ozcan *et al*, 2006; Watanabe *et al*, 2006). As such, bile acids may be an example of transgenomic mechanism of *quorum sensing* (Nicholson *et al*, 2005), whereby microbial cells communicate with each other and disperse their metabolic functions, thus behaving like a multicellular organism.

Metabolic profiling on conventional mice, compared to HBF animals, showed that the gut microflora are an essential evolutionary driver towards providing more refined control mechanisms on the host's physiology, which ultimately determine host nutritional status and health. Our results suggest that controlling the dynamics of the gut microbiome to maintain or re-establish a balanced and well-adapted microflora could help to prevent some microbial-related metabolic disorders such as hepato-gastrointestinal diseases.

Materials and methods

Animal handling procedure and probiotic administration

All animal studies were carried out under appropriate national guidelines at the Nestlé Research Center (Lausanne, Switzerland). The HBF strains were isolated from stool from a 20-day-old female baby, who was naturally delivered and breast-fed as described previously (Guigoz *et al*, 2002). The HBF flora contained only the following strains of bacteria: *E. coli, Bifidobacteria breve, B. longum, Staphylococcus epidermidis, S. aureus, C. perfringens* and *Bacteroides*. After 48 h at 37°C (24 h for *E. coli, S. aureus* and *S. epidermidis*), the number of bacteria for each strain was estimated as described previously (Guigoz *et al*, 2002) and were mixed at equal amounts (10^{10} cells/ml for each strain) for gavage. Bacterial cell mixtures for inoculation were kept in frozen aliquots with their spent culture medium until use. *L. paracasei* was obtained from the Nestlé Culture Collection (Lausanne, Switzerland) and grown under anaerobic conditions in Man-Rogosa-Sharpe (MRS) culture medium.

A total of 26 C3H female mice, aged 6 weeks, were fed with a standard pathogen-free rodent diet (Nestlé, Switzerland). A group of conventional mice was kept as control (n=9). One group of germfree mice was re-conventionalized by removal from their germfree isolator and exposure to normal environment for a period of 4 weeks (n=10). A second group of germfree mice received a single dose of HBF (n=7) by oral gavage and 2 weeks later, they were given *L. paracasei* probiotic by mixing aliquots of 1 ml probiotics (4×10^9 cells/ml) with 200 ml of saline under pathogen-free conditions for a period of 2 weeks. As each mouse drinks on average 5 ml/day, each mouse received around 10^8 probiotic bacteria per day, which allows maintaining the probiotic population in a steady state within the gut environment. Animals were euthanized after 4 weeks and microbial analysis was carried out on fecal samples as described previously (Guigoz *et al*, 2002). Urine was collected from mice before killing upon holding them by immobilization grip and urine was snap-frozen immediately. Blood (400 µl) was collected into Li-heparin tubes and the plasma was obtained after centrifugation and frozen at −70°C. The liver was dissected and snap-frozen. The intestine from the stomach to the cecum was removed from each animal. The first 1 cm length after the stomach was considered to be duodenum and the rest was divided into three sections: the first 2/3 was designated as jejunum and the remaining 1/3 as ileum. Three-centimeter samples (3 cm) were excised from the middle of each section. Ileal flush samples were obtained by rinsing the ileal lumen with 1 ml of a phosphate buffer solution (0.2 M Na_2HPO_4/0.04 M NaH_2PO_4 (pH 7.4)) using a 1-ml sterile syringe. Samples were retrieved in Eppendorf tubes and snap-frozen before NMR spectroscopy and UPLC–MS analyses. Samples included five flush samples from conventional and re-conventionalized mice and seven flush samples from HBF colonized mice. Cecal content was collected upon animal autopsy, snap-frozen immediately and kept at −80°C before analysis.

Microbial profiling of fecal contents

Briefly, for each mouse, one fecal pellet was homogenized in 0.5 ml Ringer solution (Oxoid, UK) supplemented with 0.05% (w/v) L-cysteine (HCl), and different dilution of the bacterial solution were plated on selective and semiselective media for the enumeration of specific microorganisms: *Bifidobacteria* on Eugom Tomato medium, *Lactobacillus* on Man, Rogosa and Sharpe (MRS) + antibiotics (phosphomycine, sulfamethoxazole and trimethoprime) medium, *C. perfringens* on NN-agar medium, Enterobacteriaceae on Drigalski medium and *Bacteroides* on Shaedler Neo Vanco medium (Guigoz *et al*, 2002). Plates were incubated at 37°C under aerobic conditions for 24 h for the counting of Enterobacteriaceae, and under anaerobic conditions during 48 h for *Bifidobacteria*, *Lactobacillus*, *Bacteroides* and *C. perfringens*.

Gas chromatography analysis of cecal contents

Fecal SCFAs in cecum were analyzed using gas chromatography flame-ionization-detection (GC-FID). An aliquot of cecal content was extracted with 4 ml buffer (0.1% (w/v) $HgCl_2$ and 1% (v/v) H_3PO_4) supplemented with 0.045 mg/ml 2,2-dimethylbutyric acid (as internal standard) per gram fresh weight. The resulting slurry was centrifuged for 30 min at 5000 *g* at 4°C, and the SCFAs in the supernatant collected were analyzed using a GC (HP 6890) equipped with flame ionization detector (FID) and a DB-FFAP column (J&W Scientific, MSP Friedli and Co., Switzerland) of 30 m length, 530 µm diameter and 1 µm film thickness. The system was run with helium gas at an inlet constant pressure of 10 psi at 180°C. Each sample run was preceded with a cleaning injection of 1.2% formic acid. Samples were run at an initial temperature of 80°C for 1.2 min, then at 145°C for 6.5 min, at 200°C for 0.55 min and at 200°C for 0.5 min. SCFAs were identified using external standards consisting of authentic acetate, propionate, iso-butyrate, *n*-butyrate, iso-valerate and *n*-valerate, and the concentration was calculated using internal standard.

^{1}H NMR spectroscopic analysis

Plasma samples were prepared by adding saline solution containing 10% D_2O (serving as a spectrometer field frequency lock) into 100 µl of blood plasma to a total volume of 550 µl. Urine samples were prepared by mixing 20 µl of samples with 30 µl of a deuterated phosphate buffer solution (90% D_2O, 10% H_2O) containing 0.25 mM 3-trimethylsilyl-1-[2,2,3,3-$^2H_4$] propionate (TSP) as chemical shift reference (δ 0.0). Ileal flushes were sonicated at ambient temperature (298 K) for 30 min to destroy bacterial cells and then centrifuged at 13 000 r.p.m. for 15 min. Aliquots of 300 µl were mixed with 300 µl of a solution containing 90% D_2O and 0.25 mM TSP. Intact liver samples were bathed in 0.9% saline D_2O solution. A portion of the tissue (~15 mg) was inserted into a zirconium oxide 4 mm outer diameter rotor, using an insert to make a spherical sample volume of 25 µl.

All ^{1}H NMR spectra were recorded on a Bruker DRX 600 NMR spectrometer (Rheinstetten, Germany) operating at 600.11 MHz for ^{1}H

observation. ^{1}H NMR spectra of plasma, urine and ileal flushes were acquired with a Bruker 5 mm TXI triple resonance probe at 298 K. ^{1}H NMR spectra of intact liver tissues were acquired under magic-angle-spinning conditions at a spin rate of 5000 Hz (Waters *et al*, 2000). Tissue samples were regulated at 283 K using cold N_2 gas during the acquisition of the spectra to minimize any time-dependent biochemical degradation.

1D ^{1}H NMR spectra were obtained from each sample using a standard solvent suppression pulse sequence (RD-90°-t_1-90°-t_m-90°-acquire FID) with t_m fixed at 100 ms and t_1 at 3 μs (Wang *et al*, 2005). Additional 1D Carr-Purcell-Meiboom-Gill (CPMG) spectra were acquired for plasma and liver samples. CPMG spectra were acquired using the pulse sequence (RD-90°-(t-180°-t)$_n$-acquire FID), with a spin–spin relaxation delay, $2n\tau$, of 160 ms for plasma and 200 ms for tissue (Stejskal and Tanner, 1965). The 90° pulse length was 9.0–12 μs. A total of 128 transients were collected into 32 K data points with a pulse recycle delay (RD) of 2 s.

For assignment purposes, 2D COSY (Nagayama, 1980) and TOCSY (Bax and Davis, 1985) NMR spectra were acquired on selected samples. Further assignment of the metabolites was also accomplished with the use of STOCSY on 1D spectra (Cloarec *et al*, 2005a).

UPLC–MS materials and methods

The UPLC of ileal flushes was performed on a ACQUITY UPLC™ system (Waters, Milford, MA, USA). Mass Spectrometry was performed on a TOF™ LCT-Premier (Waters MS Technologies, Manchester, UK). Flush samples were first freeze-dried before being diluted to a final concentration of 1 mg/ml with a 1:1 acetonitrile/water solution. Samples were maintained at 4°C, and 10 and 1 μl injections were made into a 10 cm × 2.1 mm ACQUITY™ BEH C18 1.7 μm UPLC column (Waters) maintained in an oven at 40°C. The bile acids eluted under gradient conditions at a flow rate of 500 μl/min from acetonitrile:water=40:60 to 60:40 over 12 min (pH 4).

The Q-TOF mass spectrometer was operated in W-optic path and negative ion mode with a capillary voltage of 2.6 kV, cone voltage of 50 V, nebulizer gas flow of 600 l/h, desolvation temperature of 300°C and a source temperature of 100°C. All analyses were acquired using the lock-spray to ensure mass accuracy and reproducibility, and leucine-enkephalin was used as the lock mass (m/z 554.2615) at a concentration of 200 ng/ml and a flow rate of 20 μl/min. Data were collected over 12 min in centroid mode with a lock-spray frequency of 11 s over the mass range m/z 50–850 with an acquisition time of 250 ms, an interscan delay of 50 ms and data averaging over 10 scans.

The standards used as bile acid reference materials are listed in Figure 4 with the abbreviations, molecular structure, molecular weight and the retention time observed using this UPLC–MS method.

Data preparation

^{1}H NMR spectra were manually phased and baseline-corrected using XwinNMR 3.5 (Bruker Biospin, Rheinstetten, Germany) and referenced to the chemical shift of the CH_3 resonance of alanine at δ 1.466. The regions containing the water resonance (δ 4.5–5.19), and for urine urea resonance (δ 4.5–6.2), were removed. The spectra were converted into 22 K data points over the range of δ 0.2–10.0 using an in-house-developed MATLAB routine (Dr O Cloarec, personal communication). The spectra were normalized to a constant sum before chemometric analyses.

UPLC–MS data were processed using the Micromass MarkerLynx™ applications manager Version 4.0 (Waters). The peaks of bile acids were identified by comparison to the m/z ratio and retention time of a set of standard bile acids (Figure 4). Integration of the UPLC–MS bile acid peaks was performed using ApexTrack2™ peak detection (Waters). Data were noise-reduced in both the UPLC and MS domains using MarkerLynx™. The ion intensities for each bile acid identified were normalized, within each sample, to the sum of the peak intensities in that sample.

Chemometrics: modeling and interpretation

Statistical analysis of the changes in bacterial populations and in the fecal composition in SCFAs obtained by GC-FID was carried out using a two-tailed Mann–Whitney test.

The multivariate pattern recognition techniques used in this study were based on orthogonal projection to latent structure (O-PLS) approach with unit-variance scaling (Trygg and Wold, 2003). In O-PLS-DA algorithm, the variation in X (NMR spectra or ion counts) is decomposed into three parts: first, the variation in X (the data matrix) related to Y (the class matrix), and the two last parts contain the specific systemic variation in X and residual, respectively (Trygg and Wold, 2003). This leads to a model with a minimal number of predictive components defined by the number of degrees of freedom between group variances. The O-PLS coefficient (covariance) plots are presented using a back-scaling transformation, which preserves the original spectral structure appearance for NMR data (Cloarec *et al*, 2005b). This also allows each data variable to be plotted with a color code, which relates to the significance of class discrimination as calculated from the correlation matrix. The covariance and correlation correspond to the shape and color code respectively. Here, a coefficient of r=0.57 was determined according to the test for the significance of the Pearson's product-moment correlation coefficient as the cutoff value, which was calculated based on discrimination significance at the level of $P<0.05$. The standard seven-fold cross-validation method was applied to establish the robustness of the model (Holmes *et al*, 2006).

Bipartite graph representation bile acid and fecal flora profiles

To explore the possible transgenomic interactions between gut microbes and the host's metabolism, functional correlation networks were derived from bile acid and fecal flora profiles correlation coefficients using the bipartite graph Rgraphsviz package from R to represent the correlation matrix. Pearson's correlation coefficients were computed between bile acid variables and fecal flora variables from the same animals. A cutoff was then applied to the absolute value of the coefficient $|r|$, so that absolute correlations $|r|>$cutoff were set to 1 and absolute correlations $|r|<$cutoff were set to 0, thus defining the adjacency matrix for the graph (defining connections between entities). Hence, $G=(N, E)$ specifies a graph G with N denoting the two node sets (two types of nodes: bile acids and fecal flora) and E the edge set (link between nodes, here a correlation between bile acids and fecal flora above the cutoff, i.e. $|r|>0.5$). The bipartite graph represents only the correlations between the two types of nodes (fecal flora and bile acids). In that context, presence of edges between two specific nodes (one of each type) reveals a functional correlation (above the cutoff) between these two entities. On the graph, the edges were then color-coded to represent the sign of the initial correlation (blue negative, orange positive) and the correlation value was displayed. To assess the pattern of correlations between fecal flora and bile acids, several correlation cutoff values were tested. For each correlation cutoff value, the number of edges connected to each was then computed to assess the degree of the network (number of edges connected to the most connected node).

Supplementary information

Supplementary information is available at the *Molecular Systems Biology* website (www.nature.com/msb).

Acknowledgements

We acknowledge Isabelle Rochat, Catherine Murset and Gloria Reuteler for microbiota analysis; Christine Cherbut and Florence Rochat for their input and help; and John Newell, Monique Julita, Massimo Marchesini, Catherine Schwartz and Christophe Maubert for their help during handling the animals. This work received financial support from Nestle to FPM, YW; INTERMAP for IKSY; Biological Atlas of Insulin Resistance Consortium under the Wellcome Trust Functional Genomics Initiative grant (066786) to OC and MED; and Roche Organ Transplantation Research Foundation for financial support to CLQ. HRT acknowledges China NSFC (20575074), the Chinese Academy of Sciences (100T program 2005[35]-T12508-O6S138) and National Basic Research Program of China (2006CB503909) for financial supports.

References

Armstrong MJ, Carey MC (1982) The hydrophobic–hydrophilic balance of bile salts. Inverse correlation between reverse-phase high performance liquid chromatographic mobilities and micellar cholesterol-solubilizing capacities. *J Lipid Res* **23:** 70–80

Backhed F, Ding H, Wang T, Hooper LV, Koh GY, Nagy A, Semenkovich CF, Gordon JI (2004) The gut microbiota as an environmental factor that regulates fat storage. *Proc Natl Acad Sci USA* **101:** 15718–15723

Backhed F, Ley R, Sonnenburg J, Peterson D, Gordon J (2005) Host-bacterial mutualism in the human intestine. *Science* **307:** 1915–1920

Bax A, Davis D (1985) MLEV-17-based two-dimensional homonuclear magnetization transfer spectroscopy. *J Magn Reson* **65:** 355–360

Bollard ME, Keun HC, Beckonert O, Ebbels TM, Antti H, Nicholls AW, Shockcor JP, Cantor GH, Stevens G, Lindon JC, Holmes E, Nicholson JK (2005) Comparative metabonomics of differential hydrazine toxicity in the rat and mouse. *Toxicol Appl Pharmacol* **204:** 135–151

Chace DH (2001) Mass spectrometry in the clinical laboratory. *Chem Rev* **101:** 445–477

Clarke SD, Romsos DR, Tsai AC, Belo PS, Bergen WG, Leveille GA (1976) Studies of the effect of dietary cholesterol on hepatic protein synthesis, reduced glutathione levels and serine dehydratase activity in the rat. *J Nutr* **106:** 94–102

Cloarec O, Dumas ME, Craig A, Barton RH, Trygg J, Hudson J, Blancher C, Gauguier D, Lindon JC, Holmes E, Nicholson J (2005a) Statistical total correlation spectroscopy: an exploratory approach for latent biomarker identification from metabolic ^{1}H NMR data sets. *Anal Chem* **77:** 1282–1289

Cloarec O, Dumas ME, Trygg J, Craig A, Barton RH, Lindon JC, Nicholson JK, Holmes E (2005b) Evaluation of the orthogonal projection on latent structure model limitations caused by chemical shift variability and improved visualization of biomarker changes in ^{1}H NMR spectroscopic metabonomic studies. *Anal Chem* **77:** 517–526

De Smet I, De Boever P, Verstraete W (1998) Cholesterol lowering in pigs through enhanced bacterial bile salt hydrolase activity. *Br J Nutr* **79:** 185–194

Dumas ME, Barton RH, Toye A, Cloarec O, Blancher C, Rothwell A, Fearnside J, Tatoud R, Blanc V, Lindon JC, Mitchell SC, Holmes E, McCarthy MI, Scott J, Gauguier D, Nicholson JK (2006) Metabolic profiling reveals a contribution of gut microbiota to fatty liver phenotype in insulin-resistant mice. *Proc Natl Acad Sci USA* **103:** 12511–12516

Dunne C (2001) Adaptation of bacteria to the intestinal niche: probiotics and gut disorder. *Inflamm Bowel Dis* **7:** 136–145

Eckburg PB, Bik EM, Bernstein CN, Purdom E, Dethlefsen L, Sargent M, Gill SR, Nelson KE, Relman DA (2005) Diversity of the human intestinal microbial flora. *Science* **308:** 1635–1638

Eyssen H, De PG, Stragier J, Verhulst A (1983) Cooperative formation of omega-muricholic acid by intestinal microorganisms. *Appl Environ Microbiol* **45:** 141–147

Floch MH (2002) Bile salts, intestinal microflora and enterohepatic circulation. *Dig Liver Dis* **34:** S54–S57

Gill SR, Pop M, Deboy RT, Eckburg PB, Turnbaugh PJ, Samuel BS, Gordon JI, Relman DA, Fraser-Liggett CM, Nelson KE (2006) Metagenomic analysis of the human distal gut microbiome. *Science* **312:** 1355–1359

Girard A, Madani S, El Boustani ES, Belleville J, Prost J (2005) Changes in lipid metabolism and antioxidant defense status in spontaneously hypertensive rats and Wistar rats fed a diet enriched with fructose and saturated fatty acids. *Nutrition* **21:** 240–248

Guigoz Y, Rochat F, Perruisseau-Carrier G, Rochat I, Schiffrin E (2002) Effects of oligosaccharide on the faecal flora and non-specific immune system in the elderly people. *Nutr Res* **22:** 13–25

Heuman DM (1989) Quantitative estimation of the hydrophilic–hydrophobic balance of mixed bile salt solutions. *J Lipid Res* **30:** 719–730

Heuman DM, Hylemon PB, Vlahcevic ZR (1989) Regulation of bile acid synthesis. III. Correlation between biliary bile salt hydrophobicity index and the activities of enzymes regulating cholesterol and bile acid synthesis in the rat. *J Lipid Res* **30:** 1161–1171

Holmes E, Cloarec O, Nicholson JK (2006) Probing latent biomarker signatures and *in vivo* pathway activity in experimental disease states via statistical total correlation spectroscopy (STOCSY) of biofluids: application to HgCl(2) toxicity. *J Proteome Res* **5:** 1313–1320

Holmes E, Nicholson J (2005) Variation in gut microbiota strongly influences individual rodent phenotypes. *Toxicol Sci* **87:** 1–2

Hooper LV, Gordon JI (2001) Commensal host–bacterial relationships in the gut. *Science* **292:** 1115–1118

Houten SM, Watanabe M, Auwerx J (2006) Endocrine functions of bile acids. *EMBO J* **25:** 1419–1425

Hurd RE (1990) Gradient-Enhanced Spectroscopy. *J Magn Reson* **87:** 422–428

Ijare OB, Somashekar BS, Gowda GA, Sharma A, Kapoor VK, Khetrapal CL (2005) Quantification of glycine and taurine conjugated bile acids in human bile using ^{1}H NMR spectroscopy. *Magn Reson Med* **53:** 1441–1446

Kibe R, Sakamoto M, Yokota H, Ishikawa H, Aiba Y, Koga Y, Benno Y (2005) Movement and fixation of intestinal microbiota after administration of human feces to germfree mice. *Appl Environ Microbiol* **71:** 3171–3178

Lederberg J (2000) Infectious history. *Science* **288:** 287–293

Ley R, Turnbaugh P, Klein S, Gordon J (2006) Microbial ecology: human gut microbes associated with obesity. *Nature* **444:** 1022–1023

Lin Y, Havinga R, Schippers IJ, Verkade HJ, Vonk RJ, Kuipers F (1996a) Characterization of the inhibitory effects of bile acids on very-low-density lipoprotein secretion by rat hepatocytes in primary culture. *Biochem J* **316** (Part 2)**:** 531–538

Lin Y, Havinga R, Verkade HJ, Moshage H, Slooff MJ, Vonk RJ, Kuipers F (1996b) Bile acids suppress the secretion of very-low-density lipoprotein by human hepatocytes in primary culture. *Hepatology* **23:** 218–228

Lorenzo-Zuniga V, Bartoli R, Planas R, Hofmann AF, Vinado B, Hagey LR, Hernandez JM, Mane J, Alvarez MA, Ausina V, Gassull MA (2003) Oral bile acids reduce bacterial overgrowth, bacterial translocation, and endotoxemia in cirrhotic rats. *Hepatology* **37:** 551–557

Martin FP, Verdu EF, Wang Y, Dumas ME, Yap IK, Cloarec O, Bergonzelli GE, Corthesy-Theulaz I, Kochhar S, Holmes E, Lindon JC, Collins SM, Nicholson JK (2006) Transgenomic metabolic interactions in a mouse disease model: interactions of *Trichinella spiralis* infection with dietary *Lactobacillus paracasei* supplementation. *J Proteome Res* **5:** 2185–2193

Mims D, Hercules D (2003) Quantification of bile acids directly from urine by MALDI-TOF-MS. *Anal Bioanal Chem* **375:** 609–616

Mims D, Hercules D (2004) Quantification of bile acids directly from plasma by MALDI-TOF-MS. *Anal Bioanal Chem* **378:** 1322–1326

Nagayama K (1980) Experimental techniques of two-dimensional correlated spectroscopy. *J Magn Reson* **40:** 321–334

Narushima S, Ito K, Kuruma K, Uchida K (2000) Composition of cecal bile acids in ex-germfree mice inoculated with human intestinal bacteria. *Lipids* **35:** 639–644

Nicholson JK (2006) Global systems biology, personalized medicine and molecular epidemiology. *Mol Syst Biol* **2:** 52

Nicholson JK, Connelly J, Lindon JC, Holmes E (2002) Metabonomics a platform for studying drug toxicity and gene function. *Nat Rev Drug Discov* **1:** 153–161

Nicholson JK, Foxall PJ, Spraul M, Farrant RD, Lindon JC (1995) 750 MHz ^{1}H and ^{1}H-^{13}C NMR spectroscopy of human blood plasma. *Anal Chem* **67:** 793–811

Nicholson JK, Holmes E, Lindon JC, Wilson ID (2004) The challenges of modeling mammalian biocomplexity. *Nat Biotechnol* **22:** 1268–1274

Nicholson JK, Holmes E, Wilson ID (2005) Gut microorganisms, mammalian metabolism and personalized health care. *Nat Rev Microbiol* **3:** 431–438

Nicholson JK, Wilson ID (1989) High resolution proton magnetic resonance spectroscopy of biological fluids. *Prog Nucl Magn Reson Spectrosc* **21:** 449–501

Ogata Y, Nishi M, Nakayama H, Kuwahara T, Ohnishi Y, Tashiro S (2003) Role of bile in intestinal barrier function and its inhibitory effect on bacterial translocation in obstructive jaundice in rats. *J Surg Res* **115:** 18–23

Ozcan U, Yilmaz E, Ozcan L, Furuhashi M, Vaillancourt E, Smith RO, Gorgun CZ, Hotamisligil GS (2006) Chemical chaperones reduce ER stress and restore glucose homeostasis in a mouse model of type 2 diabetes. *Science* **313:** 1137–1140

Palmeira CM, Rolo AP (2004) Mitochondrially-mediated toxicity of bile acids. *Toxicology* **203:** 1–15

Pereira DI, Gibson GR (2002) Effects of consumption of probiotics and prebiotics on serum lipid levels in humans. *Crit Rev Biochem Mol Biol* **37:** 259–281

Plumb RS, Granger JH, Stumpf CL, Johnson KA, Smith BW, Gaulitz S, Wilson ID, Castro-Perez J (2005) A rapid screening approach to metabonomics using UPLC and oa-TOF mass spectrometry: application to age, gender and diurnal variation in normal/Zucker obese rats and black, white and nude mice. *Analyst* **130:** 844–849

Plumb RS, Rainville P, Smith BW, Johnson KA, Castro-Perez J, Wilson ID, Nicholson JK (2006) Generation of ultrahigh peak capacity LC separations via elevated temperatures and high linear mobile-phase velocities. *Anal Chem* **78:** 7278–7283

Ridlon JM, Kang DJ, Hylemon PB (2006) Bile salt biotransformations by human intestinal bacteria. *J Lipid Res* **47:** 241–259

Sacquet EC, Gadelle DP, Riottot MJ, Raibaud PM (1984) Absence of transformation of beta-muricholic acid by human microflora implanted in the digestive tracts of germfree male rats. *Appl Environ Microbiol* **47:** 1167–1168

Sacquet EC, Raibaud PM, Mejean C, Riottot MJ, Leprince C, Leglise PC (1979) Bacterial formation of omega-muricholic acid in rats. *Appl Environ Microbiol* **37:** 1127–1131

Sonnenburg JL, Chen CT, Gordon JI (2006) Genomic and metabolic studies of the impact of probiotics on a model gut symbiont and host. *PLoS Biol* **4:** e413

Staggers JE, Frost SC, Wells MA (1982) Studies on fat digestion, absorption, and transport in the suckling rat. III. Composition of bile and evidence for enterohepatic circulation of bile salts. *J Lipid Res* **23:** 1143–1151

Stejskal EO, Tanner JE (1965) Spin diffusion measurements: spin echoes in the presence of a time-dependent field gradient. *J Chem Phys* **42:** 288–292

Tannock GW (2004) A special fondness for lactobacilli. *Appl Environ Microbiol* **70:** 3189–3194

Terahara M, Nishide S, Kaneko T (2000) Preventive effect of *Lactobacillus delbrueckii* subsp. *bulgaricus* on the oxidation of LDL. *Biosci Biotechnol Biochem* **64:** 1868–1873

Trygg J, Wold S (2003) O2-PLS, a two-block (X-Y) latent variable regression (LVR) method with an integrated OSC filter. *J Chemom* **17:** 53–64

Tugnoli V, Mucci A, Schenetti L, Calabrese C, Di FG, Rossi MC, Tosi MR (2004) Molecular characterization of human gastric mucosa by HR-MAS magnetic resonance spectroscopy. *Int J Mol Med* **14:** 1065–1071

Turnbaugh P, Ley R, Mahowald M, Magrini V, Mardis E, Gordon J (2006) An obesity-associated gut microbiome with increased capacity for energy harvest. *Nature* **444:** 1027–1031

Van Sr DS, Reeds PJ, Stoll B, Henry JF, Rosenberger JR, Burrin DG, Van Goudoever JB (2002) The high metabolic cost of a functional gut. *Gastroenterology* **123:** 1931–1940

Wang Y, Tang H, Holmes E, Lindon JC, Turini ME, Sprenger N, Bergonzelli G, Fay LB, Kochhar S, Nicholson JK (2005) Biochemical characterization of rat intestine development using high-resolution magic-angle-spinning ^{1}H NMR spectroscopy and multivariate data analysis. *J Proteome Res* **4:** 1324–1329

Watanabe M, Houten SM, Mataki C, Christoffolete MA, Kim BW, Sato H, Messaddeq N, Harney JW, Ezaki O, Kodama T, Schoonjans K, Bianco AC, Auwerx J (2006) Bile acids induce energy expenditure by promoting intracellular thyroid hormone activation. *Nature* **439:** 484–489

Watanabe M, Houten SM, Wang L, Moschetta A, Mangelsdorf DJ, Heyman RA, Moore DD, Auwerx J (2004) Bile acids lower triglyceride levels via a pathway involving FXR, SHP, and SREBP-1c. *J Clin Invest* **113:** 1408–1418

Waters NJ, Garrod S, Farrant RD, Haselden JN, Connor SC, Connelly J, Lindon JC, Holmes E, Nicholson JK (2000) High-resolution magic angle spinning ^{1}H NMR spectroscopy of intact liver and kidney: optimisation of sample preparation procedures and biochemical stability of tissue during spectral acquisition. *Anal Biochem* **282:** 16–23

Watkins JB (1985) Lipid digestion and absorption. *Pediatrics* **75** (1 Part 2)**:** 151–156

Wilson ID, Nicholson JK, Castro-Perez J, Granger JH, Johnson KA, Smith BW, Plumb RS (2005) High resolution 'ultra performance' liquid chromatography coupled to oa-TOF mass spectrometry as a tool for differential metabolic pathway profiling in functional genomic studies. *J Proteome Res* **4:** 591–598

Wu G, Fang YZ, Yang S, Lupton JR, Turner ND (2004) Glutathione metabolism and its implications for health. *J Nutr* **134:** 489–492

Xiao JZ, Kondo S, Takahashi N, Miyaji K, Oshida K, Hiramatsu A, Iwatsuki K, Kokubo S, Hosono A (2003) Effects of milk products fermented by *Bifidobacterium longum* on blood lipids in rats and healthy adult male volunteers. *J Dairy Sci* **86:** 2452–2461

Xu J, Bjursell MK, Himrod J, Deng S, Carmichael LK, Chaing HC, Hooper LV, Gordon JI (2003) A genomic view of the human–*Bacteroides thetaiotaomicron* symbiosis. *Science* **299:** 2074–2076

Xu J, Gordon JI (2003) Inaugural article: honor thy symbionts. *Proc Natl Acad Sci USA* **100:** 10452–10459